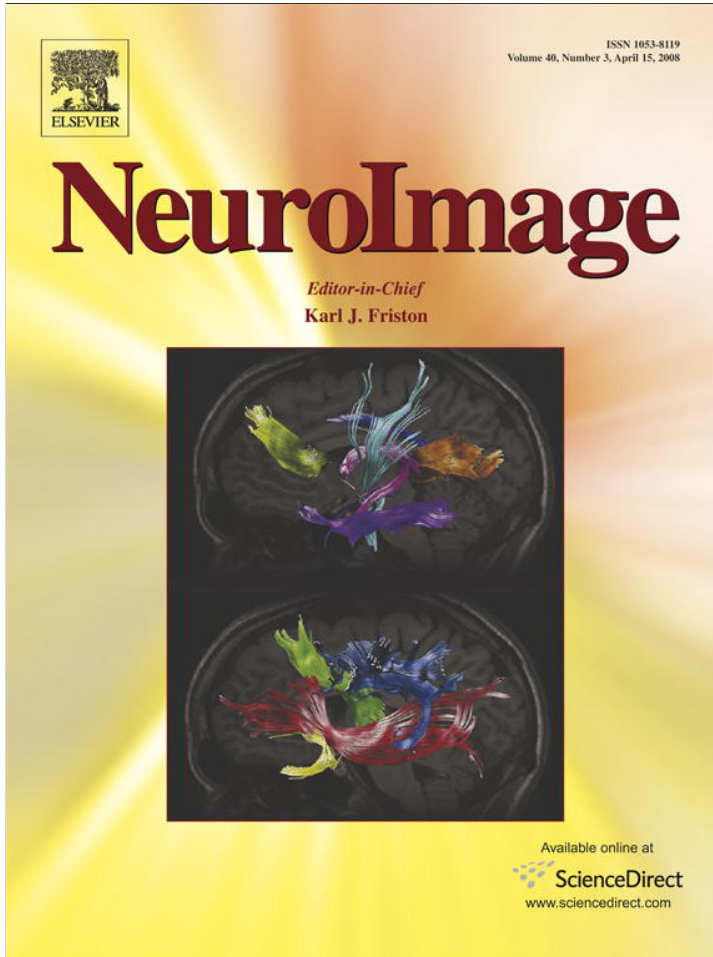


Provided for non-commercial research and education use.  
Not for reproduction, distribution or commercial use.



This article appeared in a journal published by Elsevier. The attached copy is furnished to the author for internal non-commercial research and education use, including for instruction at the authors institution and sharing with colleagues.

Other uses, including reproduction and distribution, or selling or licensing copies, or posting to personal, institutional or third party websites are prohibited.

In most cases authors are permitted to post their version of the article (e.g. in Word or Tex form) to their personal website or institutional repository. Authors requiring further information regarding Elsevier's archiving and manuscript policies are encouraged to visit:

<http://www.elsevier.com/copyright>



## Generating a model of the three-dimensional spatial distribution of neurons using density maps

Luis Cruz,<sup>a,\*</sup> Brigita Urbanc,<sup>a</sup> Andrew Inglis,<sup>a</sup> Douglas L. Rosene,<sup>b,c</sup> and H.E. Stanley<sup>a</sup>

<sup>a</sup>Center for Polymer Studies and Department of Physics, Boston University, Boston, MA 02215, USA

<sup>b</sup>Department of Anatomy and Neurobiology, Boston University School of Medicine, Boston, MA 02118, USA

<sup>c</sup>Yerkes National Primate Research Center, Emory University, Atlanta, GA 30322, USA

Received 15 October 2007; revised 22 December 2007; accepted 27 December 2007

Available online 5 January 2008

**Microcolumns are a vertical arrangement of neocortical neurons that may constitute a fundamental computational ensemble but have been difficult to study morphologically because of the challenges of determining the three-dimensional (3D) spatial arrangements of individual neurons in the ensemble.** Previously, a statistical density map method was developed to characterize microcolumns using two-dimensional (2D) coordinates of neurons from thin tissue sections. Here we extend this approach to derive the relationship between these 2D density maps and the actual 3D properties of microcolumns by creating a theoretical 3D model of cortical neurons. In seven steps, we transform a 3D initial arrangement of neurons from a crystalline lattice, with distances and neuron numbers approximating the idealized cortical microcolumn as assayed by our 2D density map analysis, into a model whose neuronal locations represent a plausible 3D arrangement of neurons in the brain. Because we constrain the transformations on the 3D model by the 2D density map properties, the transformed 3D model will exhibit properties that are consistent with experimental findings regarding microcolumnar anatomy in the brain. Moreover, because our methodology only requires the  $x,y$  locations of neurons from thin sections, it is readily accessible to any set of input data regardless of preparation or staining, from human or animals. By generating 3D model neuronal arrangements and comparing between control, aged, and diseased brain, our method can be used to test hypotheses about the effects of neurological diseases as well as normal aging on the 3D structure of microcolumns in the brain.

© 2008 Elsevier Inc. All rights reserved.

**Keywords:** Microcolumns; Minicolumns; Density map; Cerebral cortex; Primate brain; Modeling; Correlation; Neuronal organization

### Introduction

A prominent feature of the cerebral cortex is the columnar organization of cellular bodies particularly evident in Nissl-stained preparations of tissue in the temporal cortex of humans and other primates. These organized vertical neuronal structures have been termed minicolumns (Mountcastle, 1997, 2003), although they sometimes share terminology with other possibly related intracortical elements such as bundles of apical dendrites (Peters, 1994; Rockland and Ichinohe, 2004) or axons of pyramidal cells and pyramidal cell modules (DeFelipe, 1990; Jones, 2000). Physiological evidence of microcolumns may be found from tracer studies in area TE in monkey brains (Saleem et al., 1993) and studies by 2-deoxyglucose labeling in primary somatosensory cortex of monkeys and cats (Tommerdahl et al., 1993). Studies have also indicated that neurons in the microcolumn may be more interconnected than those outside the microcolumn (Constantinidis et al., 2001; Vercelli et al., 2004) and microcolumns have been proposed as a basic computational unit of the cortex (Mountcastle, 1957, 1997, 2003; Peters and Sethares, 1996; Buxhoeveden and Casanova, 2002a). On the other hand, there are other studies that indicate that this characterization of the microcolumn as a fundamental unit of organization and function is not without problems (Jones, 2000; Rockland and Ichinohe, 2004; Buxhoeveden and Casanova, 2005; Krieger et al., 2007). Even studies of “whisker columns” or barrels in the rodent somatosensory cortex, that are the anatomical equivalent of a functional cortical column, indicate that they are not a functional unit consisting of cells with similar functional properties (Helmstaedter et al., 2007). Indeed, it has recently been argued that even the very well established and much studied ocular dominance columns seem to not serve a purpose (Horton and Adams, 2005). Thus, the issue regarding the functionality of microcolumns, although debatable, is still important and relevant where the definite proof of function is an open question and one that awaits empirical confirmation (Jones, 2000; Mountcastle, 2003; Rockland and Ichinohe, 2004).

\* Corresponding author. Center for Polymer Studies, Department of Physics, 590 Commonwealth Ave, Boston University, Boston, MA 02215, USA. Fax: +1 617 353 3783.

E-mail address: [ccruz@bu.edu](mailto:ccruz@bu.edu) (L. Cruz).

Available online on ScienceDirect ([www.sciencedirect.com](http://www.sciencedirect.com)).

There are many studies concerned with properties of microcolumns and associated structures. For example, there are studies on “cellular” microcolumns (see reviews by Buxhoeveden and Casanova, 2002a,b), pyramidal cell modules (Peters and Kara, 1987; Peters and Sethares, 1991; White and Peters, 1993; Peters and Sethares, 1996; Peters, 1994; Peters, et. al., 1997), and bundles of myelinated axons (DeFelipe et al., 1990; Peters and Sethares, 1996). These studies exemplify a larger body of work that tries to understand the vertical structures in general and that provides a wealth of data related to anatomy, connectivity, and function. These data, however, fall short when addressing a crucial question: the distribution of neurons within and between microcolumns. This is an important issue as it is clear that for example the three-dimensional (3D) structural arrangement of neurons around the central bundle of apical dendrites is a critical feature of the microcolumn and its functions. Yet experimental studies of the spatial arrangements of these neurons have been hampered by many technical limitations that prevent these spatial arrangements from being studied efficiently and quantitatively. For example, one could prepare thick plastic sections in which the 3D locations of every neuron are manually marked. This preparation, however, is only practical for small studies of limited areas, preventing studies of entire cortical areas, or large subject populations. Moreover, the required thick plastic sections would have to be specially prepared as most tissue banks and brain section archives consist of thin paraffin sections (5 to 15  $\mu\text{m}$  thick), thin frozen sections (10 to 60  $\mu\text{m}$  thick), or thin celloidin sections (30 to 60  $\mu\text{m}$  thick) (see for example: [www.brainmuseum.org](http://www.brainmuseum.org) and [www.brainmaps.org](http://www.brainmaps.org)).

Several different approaches have been developed to quantify microcolumnar properties by using instead the two-dimensional (2D) coordinates of neurons obtained from widely available thin sections (Buldyrev et al., 2000; Buxhoeveden et al., 2000a; Cruz et al., 2005). These methods are of interest as they have provided evidence of changes in microcolumnar properties in a number of different conditions that suggest the potential functional significance for different microcolumnar properties. For example, there are studies of structural differences of microcolumns: across different species (Buxhoeveden et al., 2001), across different cortical areas within one species (Cruz et al., 2005) as well as in normal aging (Cruz et al., 2004), in the AD brain (VanHoesen and Solodkin, 1993; Buldyrev et al., 2000), in schizophrenia (Benes and Bird, 1987; Buxhoeveden et al., 2000b), in Down's syndrome (Buxhoeveden et al., 2002), in autism (Casanova et al., 2003), and in dyslexia (Casanova et al., 2002). In particular, the density map method (Cruz et al., 2005) uses the 2D  $x, y$  experimentally obtained coordinates of neurons to characterize microcolumns by “measures,” such as the strength of microcolumns (ratio of the density of neurons within a defined microcolumn to the density of neurons in the ROI). Other measures include the width, length, strength of periodicity of nearest neighbor microcolumns, intercolumnar distance, and the vertical distance between neurons within a microcolumn.

Despite the utility of the density map method and its ability to be applied to large samples of tissue sections including most archival brain-banked material, there is currently no clear way to determine how changes in these measures derived from 2D projections of neurons relate to the true 3D spatial locations of neurons in the brain. To address this problem, we utilize the microcolumnar measures listed above with a new modeling approach presented here to describe and construct a plausible 3D representation of microcolumns in the sampled tissues. This approach of empirical density map data and a 3D theoretical model uses as input only the experimental  $x, y$

coordinates of neurons acquired from Nissl-stained thin sections. This method takes into account  $z$ -axis tissue collapse typical in Nissl-stained thin section samples and also the fact that these thin sections, because of the intrinsic curvature of the brain, are cut at angles that are rarely normal to the surface of the brain.

In this paper, we first describe in Methods the seven steps that transform a 3D arrangement of neurons from a crystalline lattice into a spatial arrangement with the same statistical properties, as dictated by its 2D density map, as the experimentally obtained neuronal positions from tissue. Following this, in Results, we illustrate the application of the method to construct 3D arrangements of neurons using as input the density map data derived in Cruz et al. (2005) from layer III neurons of area 46 of the rhesus monkey.

## Methods

### Model construction: general remarks

A prerequisite for the method presented here is the knowledge of the measures of microcolumnarity of the system for which the 3D model of neurons will be constructed. We define these measures as the “target” (experimental) measures. The method then starts with a theoretical arrangement of neurons in 3D initially arranged in a crystalline lattice based on morphological data where neurons are individually and progressively adjusted over the course of six remaining steps to produce a 3D model that best fits the target measures. Each step is designed to affect at least one of the measures while producing only minor changes to the other measures (Table 1). After each step, we monitor the effect of that change on all of the measures of microcolumnarity of the model and adjust the magnitude of the change to match the measure from the 3D model to the target value. In general, each step consists of (i) generating  $N$  3D blocks of neurons modified by the number of steps under scrutiny (each block is denoted as one “realization”), (ii) “cutting” one thin slice through each transformed model block (to obtain  $N$  slices) at a random orientation and inclination to generate a set of 2D “sections”, (iii) applying the density map analysis to those  $N$  sections to derive one set of microcolumnar measures corresponding to that step, and (iv) comparing the microcolumnar measures from the model to the target experimental measures.

### Model construction: steps in detail

#### Step 0—starting locations

The starting configuration for the 3D model (first step) is a cube of size  $R$  containing neurons arranged in a perfect hexagonal lattice

Table 1

Correspondence between the step number, the affected parameters at that step, and the measures of microcolumnarity that either significantly change or are constraints of each step

Step No.	Affected parameters	Relevant measures
0	All variables form a perfect lattice	$P, Y$
1	Add interneurons as % of total neuronal count	$S, T, <\rho>$
2	Adjust total neuronal count to match 2D neuronal density	$<\rho>$
3	Add a random variable to $y_0$	$T$
4	Add a random variable to $d_n$	$L, Y$
5	Add a random variable to $x_n, z_n$	$S, T, W$
6	Add a random variable to $x_c, z_c$	$T, \rho(x)$

of parallel microcolumns with dimensions derived from empirical parameters (Fig. 1). These neurons correspond to the “principal” neurons or pyramidal neurons in tissue (long axon, excitatory). The hexagonal lattice is a reasonable assumption for the starting arrangement of microcolumns whose intercolumn and interneuronal distances are based on  $P$  and  $\underline{Y}$  of the target density maps (see below for details). This assumption has an experimental basis from studies of the packing of dendritic bundles and myelinated axons of pyramidal cell modules. Some of these studies demonstrated that the positions of myelinated axons, when looking at tangential sections, were regularly arranged in the monkey primary visual cortex (Peters and Sethares, 1996). Other studies reported a hexagonal spacing between bundles in area 17 of the visual cortex of rats (Peters and Kara, 1987) and monkeys (Peters and Sethares, 1991), and in the human medial prefrontal cortex (Gabbott, 2003). However, regularity in the distribution is not universal, as for example one study reported results on neuronal and bundle packing that were inconsistent with a hexagonal arrangement of bundles in the rat primary somatosensory cortex (Skoglund et al., 2004). For this reason, the model also allows for the hexagonal lattice to be randomized (see step 6 below) to accommodate other less regular arrangements of microcolumns, thus allowing the model to depart from a perfect hexagonal lattice where the degree of randomization is dictated by the experimental density map measures, as described below.

The microcolumns are initially located at the vertex positions  $(x_c, z_c)$  of a hexagonal lattice with spacing  $d_c$  and the neurons at positions  $(x_n, y_n, z_n)$ . At this step, the set of  $(x_n, z_n)$  coincides with the set of  $(x_c, z_c)$ . Along the vertical direction, the neurons are separated by the same distance  $d_n$ . Thus defining the component  $y_n$  of their positions by

$$y_n = y_0 + m \cdot d_n, \quad (1)$$

where  $y_0$  is a constant that is the same for all microcolumns and  $m$  is an integer (Fig. 1).

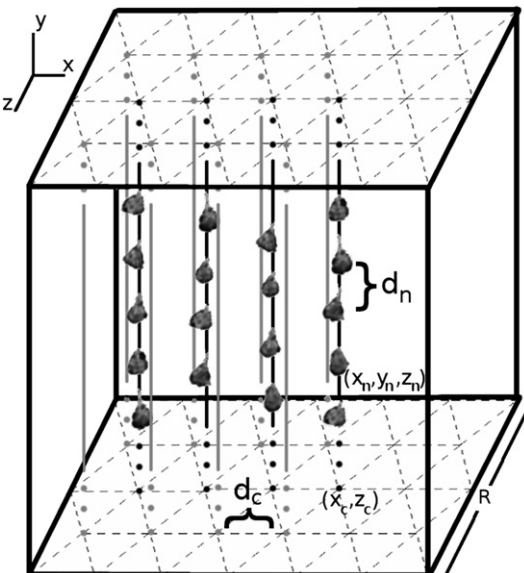


Fig. 1. Schematic diagram showing the variables in the model. The dotted lines form the hexagonal lattice on which microcolumns are initially positioned. The neuronal bodies used in the diagram only serve for illustration purposes, as in the model each neuron is represented by a sphere with the radius listed in Table 2.

The values for  $d_c$  and  $d_n$  are derived from the target density maps. Specifically, the value of  $d_c$ , the center-to-center distance between microcolumns is determined from the microcolumnar measure  $P$  corrected to take into account 3D effects (see Cruz et al., 2005, Fig. 8D). The value of  $d_n$ , the interneuron distance within microcolumns, is determined from the position of the first peak of the graph of the neuronal density along the vertical axis of the microcolumn,  $\underline{Y}$  (see for example Cruz et al., 2005, Fig. 4) corrected by the angle at which the tissue slices are cut in the model system. This correction is derived by considering that  $\underline{Y}$  is the result of averaging over many experimentally obtained thin slices cut at slightly different inclinations, or in terms of the model, at different azimuthal angles  $\phi$  (this angle is defined in Generating thin slices). An approximate relationship between  $\underline{Y}$  and  $d_n$  is then given by

$$\int_0^{\pi/3} d_n \cdot \cos\phi \, d\phi = \underline{Y}, \quad (2)$$

where we are averaging over the trigonometric projection of  $d_n$  on the vertical axis and the limits for  $\phi = [0, \pi/3]$  are taken as reasonable limits for the range of cuts in the inclination of the tissue (see Generating thin slices for an explanation).

Regarding the size of the cube  $R$ , there is no requirement on its value except that it should be big enough to contain slices cut at arbitrary orientation and inclination. For simplicity, we consider the value of  $R$  to be the diameter of the smallest sphere that can contain a cube of the size of our experimental ROI denoted by  $l$ . Then, considering a tissue slice with thickness  $s$ , the size of our block will be

$$R = 2 \cdot \sqrt{(2(l/2)^2 + (s/2)^2)}. \quad (3)$$

#### Step 1

In step 1, a number of “interneurons” are added at random positions throughout the block. These neurons correspond to non-pyramidal neurons in tissue (short axon, mainly inhibitory) for which their positional randomness assumes that they do not organize into microcolumns. For simplicity, at this step we approximate neurons as spheres with a fixed value for their radius that should correspond to the average size of neurons in the tissue. These interneurons are then added under an algorithm that first generates a random  $(x, y, z)$  location for placement and then accepts the location provided the distance between the center of the interneuron and any of the already present neurons in the system is bigger (no overlap) than twice the amount of its radius. If the position is rejected, another is generated until a suitable location is found. We note that a more realistic model could incorporate the experimentally available size distribution of neurons, but based on the neuronal sizes and densities that we have tested, using the average size of neurons is sufficient for proper placement of interneurons. In more general terms, a sphere with radius equal to the average neuronal size of the size distribution is a suitable approximation as long as the average and square root of the variance of the size distribution are much smaller than the intercolumn distance. Step 1 is only constrained by the interneuron population percentage.

#### Step 2

In step 2, the volume density of neurons is adjusted to match the experimentally measured 2D neuronal density found in the tissue sections,  $\rho$ . Specifically, a match between the 2D neuronal density of the model (from cutting thin slices, see next section) and the 2D target neuronal density is done. Because the initial crystalline block will

always have a higher density than the density found in tissue because of its higher packing fraction, the neuronal density in the model is adjusted by deleting a percentage of neurons at random (from both, principal and interneurons) from the block of model neurons.

#### Steps 3 and 4

In steps 3 and 4, randomness is introduced in the vertical arrangement of neurons. Specifically, in step 3,  $y_0$  is modified from being a constant to be a number taken from a uniform random distribution

between [0,1] multiplied by the interneuron distance in the vertical direction,  $d_n$ . This means that now individual microcolumns will be assigned a value for  $y_0$  that ranges between 0 and  $d_n$ . This step has the effect that neurons within the same microcolumns will be shifted up or down, and neurons from different microcolumns will no longer be “in-step” with one another horizontally. This step is justified by the fact that neurons in tissue indeed do not align horizontally across microcolumns. Step 3 is not constrained by any of the *target* measures. In step 4, we introduce randomness in  $d_n$ , the distance between neurons

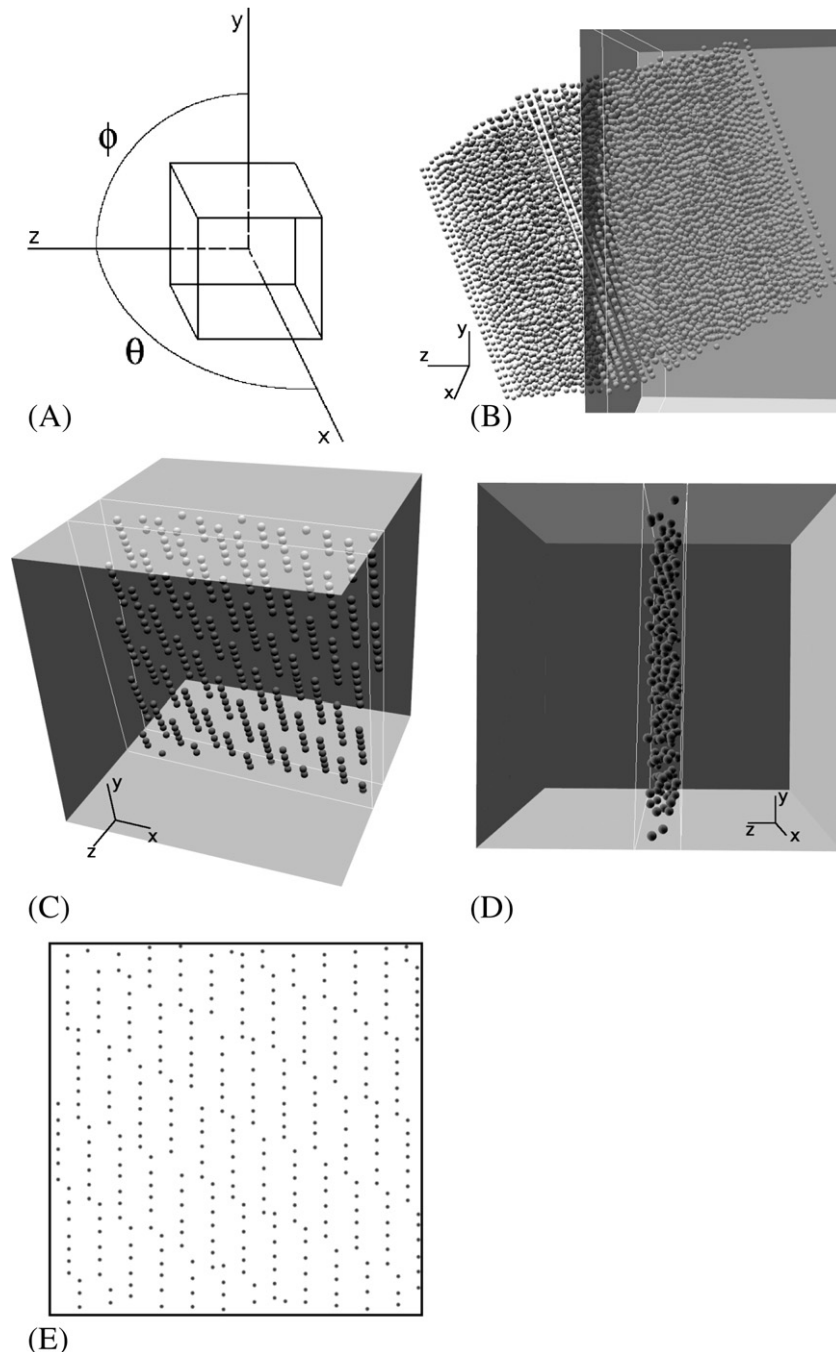


Fig. 2. Schematic diagram and example figures showing the rotation and cutting of one realization of the model neuronal block. (A) shows the axis and angles of rotation in relation to the 3D block of neurons indicated by the cubic wire box. (B) shows a rotated example of a 3D block of neurons where the neurons within the slab indicated by the thin lines are cut in (C) and (D). (E) shows the neurons from (D) collapsed into the x–y plane that is used to calculate the density maps. For visual clarity, the example shown is generated using steps only up to step 4.

within each microcolumn. Specifically, the original distances where the position of the  $i+1$  neuron relative to the  $i$ th neuron is

$$d_n^{i+1} = d_n^i + d_n \quad (4)$$

are transformed to

$$d_n^{i+1} = d_n^i + d_n + \delta d_n, \quad (5)$$

where  $\delta d_n$  is a random variable taken from a Gaussian random distribution centered at 0 and of width  $\sigma$ . A Gaussian random distribution was a necessary choice over a simple random distribution in order to obtain the shape of the curve found in Fig. 4 of Cruz et al. (2005). The value of  $\sigma$  in step 4 is determined by values of  $L$  and the shape of the curve for  $d_n$ .

#### Steps 5 and 6

In steps 5 and 6, randomness is introduced in the positions of the neurons within the horizontal  $x-z$  plane by transforming  $x_n$  to  $x_n + \delta x_n$  and  $z_n$  to  $z_n + \delta z_n$  and in the positions of each microcolumn by transforming  $x_c$  to  $x_c + \delta x_c$  and  $z_c$  to  $z_c + \delta z_c$ , respectively. The

parameters  $\delta x_n$ ,  $\delta z_n$ ,  $\delta x_c$ , and  $\delta z_c$  are variables taken from a uniform random distribution. We note that in step 5 the vertical coordinates of the model neurons  $y_n$  do not need to be corrected since they were implicitly randomized when performing step 3 in the randomization of  $y_0$ . The parameters  $\delta x_c$  and  $\delta z_c$  introduce randomness in the positions of the microcolumns having as a consequence that the structure of the underlying hexagonal lattice is reduced, with the potential to destroy all regularity depending on the values of randomness. The range of values for the set of  $(\delta x_n, \delta z_n)$  in step 5 are determined by the width,  $W$ , of the microcolumns. The range of values for the set of  $(\delta x_c, \delta z_c)$  in step 6 are determined by the broadness of the nearest-neighbor peak in the density map, measured by analyzing the neuronal density perpendicular to the axis of the microcolumn,  $\rho(x)$ .

#### Generating thin slices

A key procedure in the model is the comparison between the density maps derived from the model and those derived from experiment

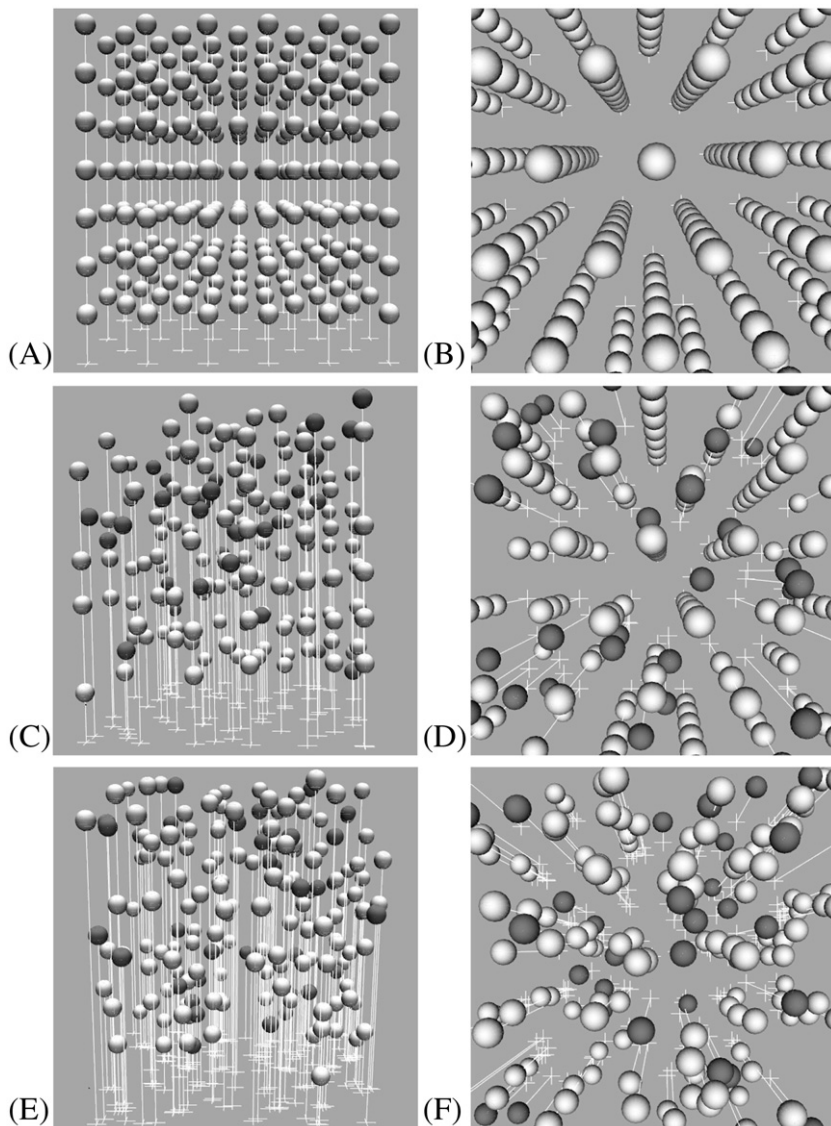


Fig. 3. Front and top view of examples of configurations at step 0 (A and B), at step 3 (C and D), and at step 6 (E and F). The darker spheres are interneurons. Each neuron has a vertical thin line whose base in the  $x-z$  plane is indicated by a thin cross.

that allows for the tuning of the adjustable model parameters to match the *target* measures at each individual step. For this comparison to happen, we need to generate “thin slices” from the 3D model from which to calculate density maps in the same way that it is done experimentally.

The procedure to “cut” the 3D model into thin slices is as follows. A 3D block is rotated by an angle  $\theta$  chosen at random in the  $x$ - $z$  plane with a range in allowed values between 0 and  $2\pi$  (Fig. 2A). Next, the block is rotated by the azimuthal angle  $\phi$  chosen at random in the  $y$ - $z$  plane (Fig. 2A) with a range in values between 0 and  $\pi/3$ , where in this work this particular maximum value for  $\phi$  is taken as a reasonable approximation for the upper bound instead of the maximum of  $\pi/2$  that would provide undesirable tangential cuts of microcolumns. These

ranges of values for rotations mimic the experimental setup where orientation and inclination angles are not fixed at the moment of acquisition of the thin-slice tissue sections but still correspond to sections that are approximately orthogonal to the pia surface and hence not tangential. An example of these rotations is given in Fig. 2B where it is shown how we select a thin slice (white wire box) from a rotated block. The “cut” thin slice is seen at an angle in Fig. 2C and from the side in Fig. 2D. Because of the rotations, the thin slice usually crops the microcolumns to an unspecified length. This means that the microcolumns in the model will appear shorter due to oblique cuts, which is also the case in experiments that measure  $L$  (Cruz et al., 2005).

Once the thin slice is obtained (Fig. 2D), all of the  $z$  coordinates are projected to the  $x$ - $y$  plane (of the reference system), which does

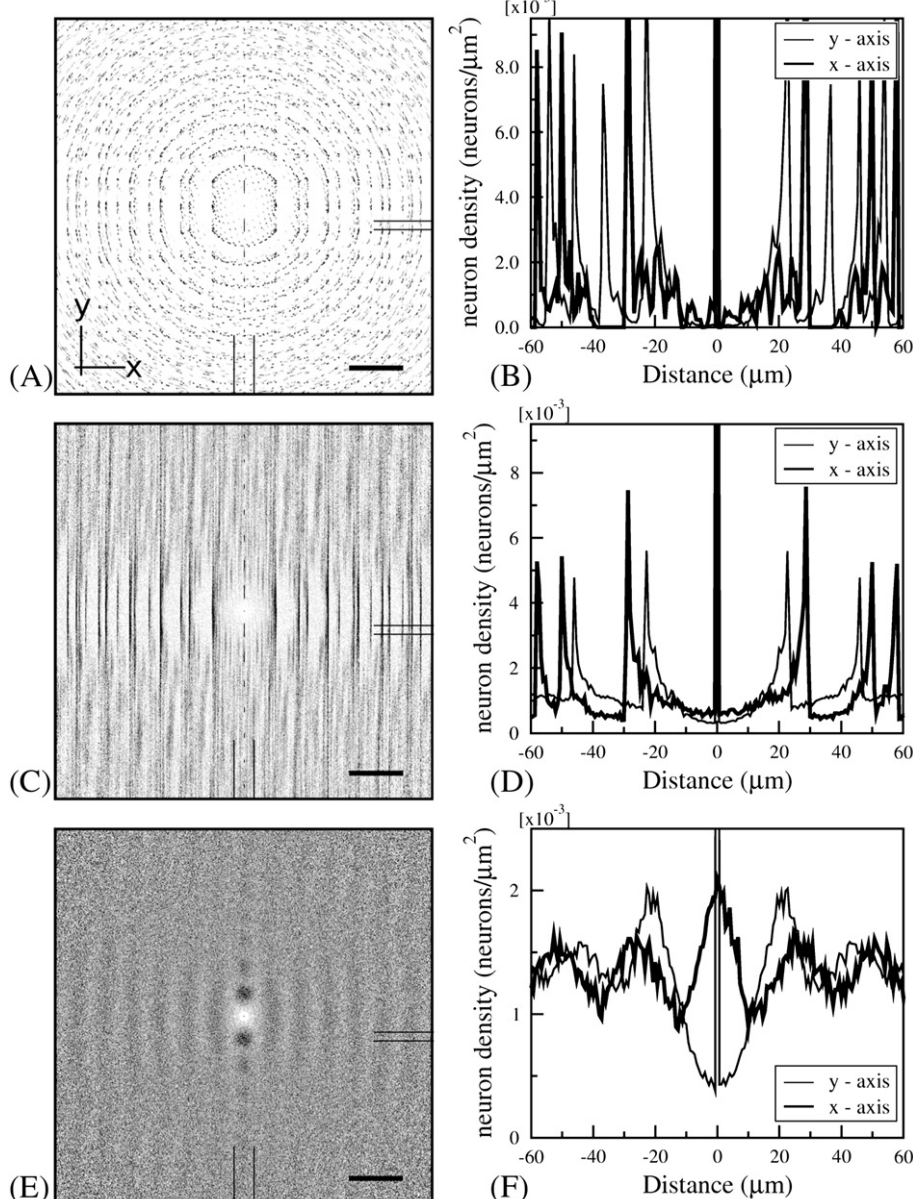


Fig. 4. Density maps given by  $g(x,y)$  in (A), (C), and (E) and respective cross-sections in (B), (D), and (F) at three of the seven steps. The density maps (A), (C), and (E) correspond to steps 0, 3, and 6, respectively. The cross-sections are calculated by measuring the neuronal density found in a strip along the thin black lines indicated in each density map. The  $y$ -axis cross-sections go through the middle of the density map while the  $x$ -axis cross-sections do not. The scale bars at the lower right corner of the density maps represent 50  $\mu$ m.

Table 2  
Values used for the three-dimensional reconstruction

Tissue property or measurement	Value
Model parameter	Value
$\underline{Y}$ , average interneuron distance.	20.0 $\mu\text{m}$ ( <sup>1</sup> ) (estimated)
$\underline{P}$ , average intercolumn distance.	26.1 $\mu\text{m}$ ( <sup>1</sup> )
$\rho$ , slide neuronal density	0.0013 neurons/ $\mu\text{m}^2$ ( <sup>1</sup> )
$l$	341 $\mu\text{m}$ ( <sup>1</sup> )
$s$ , thickness of the thin slice	30 $\mu\text{m}$ ( <sup>1</sup> )
Radius or neurons (average)	5 $\mu\text{m}$
% interneurons	20% ( <sup>2</sup> )
$d_n$ , interneuron distance.	23.1 $\mu\text{m}$
$d_c$ , intercolumn distance.	29 $\mu\text{m}$
$\theta$	Uniform random [0, $2\pi$ ]
$\phi$	Uniform random [0, $\pi/3$ ]
% omitted neurons	40%
$\delta d_n$	Gaussian distribution, $\sigma = 4.7 \mu\text{m}$
$\delta x_n, \delta z_n$	Uniform random [-6 $\mu\text{m}$ , 6 $\mu\text{m}$ ]
$\delta x_c, \delta z_c$	Uniform random [-6 $\mu\text{m}$ , 6 $\mu\text{m}$ ]
$N$ , number of images for average.	500

(<sup>1</sup>) Cruz et al., 2005; (<sup>2</sup>) Hendry et al., 1987.

not alter the  $x$ - $y$  coordinates of the neurons. This creates a 2D field of  $x$ - $y$  locations (Fig. 2E) similar to those from thin tissue sections in which neuron locations are collapsed into the plane of the slide both by shrinkage in the  $z$ -axis and by the optical depth of field when sections are digitized. We note that because the location and not the diameter of the neurons enters into the selection of neurons inside the slide, there is no ambiguity on whether neurons close to the plane of the cut belong inside or outside of the slide as may occur in experimental sections.

#### Density map method

The density map method was initially described by Buldyrev et al. (2000) and a more detailed description and validation was given by Cruz et al. (2005). Briefly, the density map method calculates the density correlation function,  $g(x,y)$ , using as input the  $(x,y)$  neuronal coordinates from an image. This function  $g(x,y)$  can be mapped to a 2D grayscale image in which different shades of gray are proportional to the average local neuronal density. Thus, the density map represents the average neuronal neighborhood surrounding every neuron within an ROI. We quantify the microcolumnar structure by extracting the following measures (Cruz et al., 2005):

- $W$ , microcolumnar width,
- $P$ , distance between microcolumns,

- $L$ , effective length (vertical span) of microcolumns,
- $S$ , strength of microcolumns (ratio of the neuronal density within a microcolumn to the average neuronal density),
- $T$ , strength of nearest neighbor microcolumns (ratio of the neuronal density of neighboring microcolumns to the average neuronal density; also measures degree of microcolumnar periodicity),
- $Y$ , distance between neurons within a microcolumn (perpendicular to pia and parallel to microcolumns—not explicitly defined, but contained, by Cruz et al., 2005).

#### Results

In this section, we present an application of the 3D modeling method by using as input previously calculated density maps derived from images of layer III, area 46, of rhesus monkey brains (Cruz et al., 2005). This application also serves as a tutorial on how to generate 3D neuronal ensembles from any set of density map measures.

During the process of the specific 3D construction below, we will refer to Fig. 3 for illustrations of the resulting 3D structures and to Fig. 4 for their corresponding density maps. In Table 1, we list those measures that are either constraints or change as a consequence of a particular step, and in Table 2, we list the experimental values used to build the model as well as the resulting values of the parameters of the model that are obtained from the match to the target values. In Table 3, we list each step (first column) along with its corresponding measures of microcolumnarity (rows). The target values coming from experimental results are given in the last row of Table 3 (row Experiment).

To provide statistics in the comparison between the model and target,  $N$  blocks of model neurons are generated after each step from which we get  $N$  model thin slices. We note that since the steps involve random numbers, no two 3D blocks will have neurons at exactly the same  $(x,y,z)$  coordinates, thus the procedure creates a set of  $N$  distinct blocks. The  $N$  blocks are then separated into  $n$  groups from which  $n$  average density maps are calculated with corresponding  $n$  sets of measures of microcolumnarity. From these  $n$  sets of model measures, one set of average (plus standard deviation) measures of microcolumnarity are calculated for the model that is compared with the corresponding experimental target measures of microcolumnarity. Because the value of the standard deviations in the measures of microcolumnarity of the model depends on  $N$  and  $n$ , which both can be made arbitrarily big (only bounded by simulation time), the value of the error in the model is only presented here as a guide and not as a true comparison with the experimental error bars. In the present work, we take  $N=500$  and divided this into  $n=5$  groups of 100.

For convenience, we define the building and modification of neuronal positions up to a given step to obtain  $N$  3D structures, the

Table 3  
Values for the microcolumnar measures

Step	$S$	$T$	$W$ ( $\mu\text{m}$ )	$P$ ( $\mu\text{m}$ )	$L$ ( $\mu\text{m}$ )	$Y$ ( $\mu\text{m}$ )	$\rho$ (neurons/ $\mu\text{m}^2$ )
0	2.14±0.06	2.08±0.14	3.17±0.01	24.0±3.3	151.2±17.6	22.1±0.3	0.0018±7×10 <sup>-6</sup>
1	1.70±0.07	1.61±0.04	3.14±0.02	23.1±3.2	147.0±26.5	20.3±3.0	0.0023±1×10 <sup>-5</sup>
2	1.70±0.04	1.66±0.07	3.15±0.03	27.9±0.9	179.8±62.3	22.3±0	0.0013±8×10 <sup>-6</sup>
3	1.64±0.04	1.17±0.01	3.18±0.02	27.1±1.4	154.2±47.8	22.2±0.2	0.0014±1×10 <sup>-6</sup>
4	1.70±0.01	1.16±0.02	3.19±0.01	27.5±0.8	35.7±18.0	21.0±0.6	0.0014±8×10 <sup>-6</sup>
5	1.21±0.02	1.09±0.01	12.89±0.85	26.4±0.6	22.3±6.3	20.7±0.7	0.0014±5×10 <sup>-6</sup>
6	1.26±0.04	1.04±0.01	13.99±0.74	26.2±1.2	23.6±7.8	21.5±0.3	0.0014±6×10 <sup>-6</sup>
Experiment	1.25±0.06	1.04±0.03	12.8±2.90	26.1±2.8	16.9±9.9	21.4±1.4	0.0013±0.0003

Shading denotes significant changes from the previous step.

*generating phase*, and the rotating and cutting of these 3D structures into thin slices, plus the calculation of their density map along with the determination of measures of microcolumnarity from this density map, the *processing phase*.

#### Step 0

The size of the block to accommodate the size of our experimental ROI ( $341 \times 341 \mu\text{m}^2$ ) is given by Eq. (3) to be about  $484 \times 484 \times 484 \mu\text{m}^3$ . A block of this size usually contains more than 7000 neurons. As described in Methods, at step 0 an initial crystalline lattice is built. The only two parameters necessary to define this initial lattice are  $d_c$  and  $d_n$ . As presented in Methods, the value of  $d_c$  is closely related to  $P$ . For our specific application of layer III microcolumns, we use a value for  $d_c$  of 29  $\mu\text{m}$  (from Cruz et al., 2005, Fig. 8D). We note that this value is of the same order of magnitude as values found in the literature for the distance between dendrite bundles, a natural measure for distances between microcolumns, in, for example, the mouse primary motor cortex bundles of layer V apical dendrites measured at the level of layer IV on average at 31  $\mu\text{m}$  apart (Lev and White, 1997), layer IV of the rat primary somatosensory cortex on average at 49  $\mu\text{m}$  apart (Skoglund et al., 2004), and the monkey visual cortex in layer IV of area 17 at about 30  $\mu\text{m}$  apart (Peters and Sethares, 1991) and between bundles of myelinated axons in layer IVc (and apical dendrites) at 23  $\mu\text{m}$  apart (Peters and Sethares, 1996). Also, in supragranular layers of the rat, primary visual cortex bundles were found to be about 27  $\mu\text{m}$  apart (Vercelli et al., 2004).

For the value of  $d_n$ , we solve for  $d_n$  in Eq. (2) and by taking  $Y=20 \mu\text{m}$  (lower bound estimate; Cruz et al., 2005, Fig. 4), we obtain  $d_n=23.1 \mu\text{m}$ . An example of an initial lattice is shown in Figs. 3A and B. After the *generating phase* up to step 0 and the *processing phase*, we obtain the density map shown in Fig. 4A along with the measures of microcolumnarity plus the average neuronal density listed in the first row of Table 3 (row 0). It can be seen by simple inspection that the density map ( $g(x,y)$  plotted in Fig. 4A) has almost no features that resemble the *target* density map (Cruz et al., 2005, Fig. 3). The cross-sections along the  $x$ - and  $y$ -axis of the model density map (Fig. 4B) show very large and discrete peaks characteristic of crystalline lattices.

#### Step 1

In step 1, interneurons are added to the system as described in Methods. Here, the radius of neurons is taken as 5  $\mu\text{m}$  where this number is derived from the average size of neurons in our tissue samples from area 46, layer III (Cruz et al., 2005). Interneurons are added to the system such that they make a total of 20% of the total number of neurons in the model system (Hendry et al., 1987). Carrying out the *generating phase* up to step 1 with the subsequent *processing phase* shows that both  $S$  and  $T$  were changed, as shown in Table 3, step 1. The significant decrease in  $S$  and  $T$  is due to the increased average density of neurons in the system because the random placement of these neurons adds more neurons outside the microcolumn than within the microcolumn.

#### Step 2

In step 2, as described in Methods, a percentage of all neurons are deleted to match the 2D neuronal density of the model system and the 2D experimentally observed density. For our specific application, we need to delete 40% of all neurons. After this reduction, the

percentage of interneurons vs. principal neurons is unchanged but the model density for 2D slices matches the experimental value without altering any of the other microcolumnar properties relative to step 1 (Table 3, step 2). The resulting density map up to step 2 (not shown) remains very close to the one shown for step 1 in Fig. 4A.

#### Step 3

In step 3, the randomization of  $y_0$  produces a radical change in the appearance of the system as illustrated in Figs. 3C and D since neurons across microcolumns no longer coincide at their  $y_n$  positions. However, the neurons within microcolumns still form perfectly spaced vertical columns, as seen in Fig. 3D (dark spheres are interneurons). After the *generating* up to step 3 and *processing phases*, we obtain the density map shown in Fig. 4C with the corresponding cross-sections in Fig. 4D. This density map shows how the periodicity in the  $y$  direction is lost and the cross-section in the  $x$ -axis shows the emergence of wider peaks for the nearest neighbor microcolumns. As shown in Table 3, while step 3 radically changed the 3D structure of the block, it only affected  $T$ , the measure of strength of neighboring microcolumns, by reducing it as immediately adjacent neurons are on average more dispersed.

#### Step 4

In step 4, after the *generating phase* up to step 4 plus the *processing phase*, we see that adding  $\delta d_n$  in Eq. (5) does not change the resulting density map (not shown, but similar to Fig. 4C) but transforms the sharp peaks in the  $y$ -axis of Fig. 4D into the smoother curves of its corresponding cross-sections (not shown, but with a  $y$ -axis similar to that of Fig. 4F) that approximate the  $y$ -axis cross-section found in the experiment (Cruz et al., 2005, Fig. 4). A value for the width of the Gaussian distribution of  $\delta d_n$  of  $\sigma=4.7 \mu\text{m}$  was enough to match these two curves. As shown in Table 3, adding  $\delta d_n$  did not affect significantly most of the measures except  $L$  and  $Y$ , both of which were brought to values closer to the *target*. The decrease in  $L$  (the vertical span of the microcolumn) comes from its definition as the length scale in an exponential envelope of the peaks in the  $y$ -axis cross-section. Smaller and smoother peaks yield a faster decay of the exponential envelope, thus a smaller  $L$ .

#### Step 5

In step 5, the random displacements of neurons in the  $x$ - $z$  plane by the addition of the random variables  $\delta x_n$  and  $\delta z_n$ , result in microcolumns with a non-zero width  $W$ , as shown in Table 3, step 5. Values for  $\delta x_n$  and  $\delta z_n$  in the range of  $\pm 6 \mu\text{m}$  were enough to match  $W$  from the model to its *target* of 12.8  $\mu\text{m}$  (from Cruz et al., 2005). These displacements introduce additional reductions in  $S$  and  $T$ . Both of these reductions happen because some neurons are displaced considerably far from the center of the microcolumns and no longer contribute to the density map-defined “microcolumn” thus weakening their microcolumnar measures from the previous step.

#### Step 6

Finally, in step 6, the positions of the base of the microcolumns are moved in random directions away from the vertices of the underlying hexagonal lattice. After the *generating* and *processing phases*, we obtain a density map (Fig. 4E) with cross-sections shown in Fig. 4F. This step broadens and lowers the peaks in the model cross-section (other than the central peak) along the  $x$ -axis

(Fig. 4F), an effect already present but of less magnitude in step 5, that match with the experimental curve when  $\delta x_c$  and  $\delta z_c$  are in the range of  $(-6 \mu\text{m}, 6 \mu\text{m})$ . This step is also essential to bring additional realism to the model, as seen by comparing Figs. 3D and F in which the regular patterns of the underlying idealized hexagonal lattice are diminished. By examination of Table 3, step 6 shows that the value of  $\underline{T}$  (strength of neighboring microcolumns) is the only measure that is significantly affected by this step.

As a result of the transformations described above, a final set of 3D blocks that best approximate the actual microcolumn organization of neurons from layer III in area 46 is obtained. A step-by-step illustration of this particular process is summarized in Fig. 5 where the measures of microcolumnarity are plotted as a function of step number. The last point in each graph corresponds to the *target* values. Significant decreases in  $\underline{S}$  toward its *target* occur at steps 1 and 5, in which interneurons and planar displacements of neuronal positions are incorporated, respectively.  $\underline{T}$  is significantly reduced toward its *target* at steps 1 (interneurons are added) and 3, in which the periodicity across microcolumns is reduced smearing the effect of nearest neighbor columns.  $W$  increases significantly as neurons are displaced in the  $x$ - $z$  plane, thus giving width to the columns. The distance between microcolumns  $P$  does not suffer any significant

change at any step. This is because the only step that could possibly affect it, step 6, only broadens and decreases the first peak of the cross-section in the  $x$ -axis (Fig. 4F) but does not change the average position of the nearest neighbor microcolumns, thus preserving the value of  $\underline{P}$ .  $L$  decreases abruptly at step 4 when the decay in the density map cross-sections increases, thus truncating  $L$ . The value for  $Y$ , the vertical distance between neurons within microcolumns, does not change appreciably except at step 4 when the distances between neurons change from being a constant to being values generated from a distribution. All of these changes along with the step number at which they occur are listed in Table 1. We note that the significant changes in the measures at particular steps, shown as big jumps in Fig. 5, will also appear at the same step number when using other data from measures of other cortical areas, but the magnitude of the changes will be dependent on the input data.

Comparing the values of the microcolumnar measures after step 6 with the *target* values (last two rows of Table 3), we observe that most of the values derived from the model were less than 8% from the values of the *target* except for  $\underline{W}$  and  $\underline{L}$  where intrinsic large fluctuations in these measures prevented a better fit. However, even for these two measures, the values from the model were within the experimental error of the  $\underline{W}$  and  $\underline{L}$  target values.

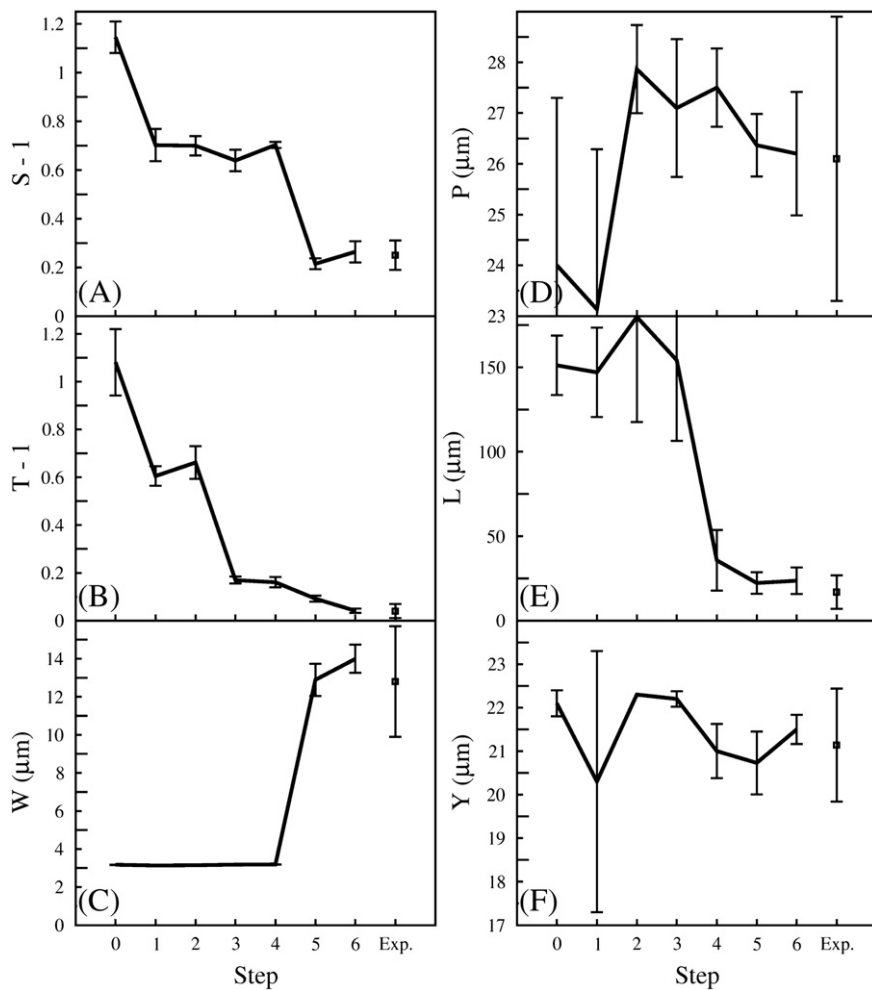


Fig. 5. Density map measures (A)  $\underline{S}$ , (B)  $\underline{T}$ , (C) width  $\underline{W}$ , (D) intercolumn distance  $\underline{P}$ , (E) length  $\underline{L}$ , and (F) interneuron distance within a microcolumn  $\underline{Y}$  as a function of step number. The last disconnected data point in each graph indicates the *target* value derived from experiment. For  $\underline{S}$  and  $\underline{T}$  we subtract one to plot the excess neuronal density above the average global neuronal density in the samples.

## Discussion

### Summary

A method is presented that starting from density maps empirically derived from the two-dimensional  $x,y$  coordinates of neurons from thin sections constructs a set of theoretical three-dimensional representations of those neurons. The method transforms, by a series of steps, a 3D crystalline lattice of neurons into a 3D spatial model configuration that gives microcolumnar measures consistent with those calculated from thin tissue sections.

### Caveats

The main limitation of our model is that it cannot generate an exact rendering of individual neuron locations given a set of 2D tissue sections since the density maps are statistical properties of such sections that can only provide average spatial properties. The model provides instead a set of  $N$  3D structures that when taken together, have the same statistical properties (density maps) as those derived from neurons in tissue. Moreover, since the  $N$  3D structures are statistically equivalent, any of them can be taken as representative of the biological system used to generate them.

There are two other important questions that remain concerning the validity of this model: (i) whether the steps involved in modifying the crystalline lattice produce a statistically “unique” representation, and (ii) whether these steps are the only way to achieve this representation.

First, regarding uniqueness of the 3D model solution, there are enough experimental constraints provided by the neuronal density and microcolumnar measures that the 3D microcolumnar arrangement that results from our specified construction and corrections is the only possible outcome that optimally matches all of the *target* experimental properties. Also, the specific sequence of steps should not influence the final configuration. However, because here we sequentially apply the steps without returning to previous steps (in a linear fashion), this may introduce errors since at every step there are minor changes to all measures (Table 3), although these changes are not significant. Instead, an algorithm in which the differences between the measures of microcolumnarity from the model (tuned by all of the adjustable parameters of the model) and those from the *target* are iteratively minimized might provide a slightly “better fit” between the 3D representation and experiment. However, this “better fit” would only bring second-order corrections (less than 1%) that would not substantially change the final parameters presented here while at the same time increasing significantly the computational effort involved in such a feedback minimizing algorithm.

Second, our choice of transforming steps is not the only way to derive an underlying 3D model as they depend (by design) upon the initial configuration. Thus instead of a perfect 3D lattice as a starting point, a set of randomly placed neurons (or columns) could have been used as the initial configuration that is then moved by a different set of steps to cause coalescence into the final microcolumnar arrangement that yields the required *target* values. However, starting from an ordered lattice that undergoes specified transformations is more amenable to systematic analysis and may yield more insight when studying changes to these transformations relative to observed alterations in development, aging, and disease.

### Potential applications

Our model is relevant to studies that assess the level of organization of neurons in the cortex over a number of variables or conditions, such as across species or between different areas of the cortex, but may be particularly useful in assessing changes across the life span. Specifically, our model could contribute to questions about when and how microcolumns emerge in development and change up to adulthood. Likewise, it is applicable to study how microcolumns change in adulthood as the brain ages (Cruz et al., 2004). For example, building a 3D model of the neuronal locations and their changes in the aging brain could help generate testable hypotheses about the underlying mechanisms and functional consequence for cortical information processing. Also, this method is relevant to studies of neurological diseases in that it can provide a unique perspective into the degree of 3D organization or disorganization in developmental disorders and in neurodegenerative diseases that affect the cortex, for example in the cross-correlation between thioflavine S-positive plaques and neurons in AD (Urbanc et al., 2002).

On a more practical level, this method offers an alternative to manually acquiring the 3D positions of cells from serial sections of 3D tissue blocks and entails a much lower cost in labor and a savings in material by deriving 3D information from the relatively common Nissl-stained sections available from many collections of brain samples (e.g. brainmaps.org). This is especially true as massive amounts of data in the form of  $x,y$  coordinates from such tissue can now be automatically obtained using a recently developed automatic neuronal recognition method based on a combination of image segmentation and machine learning (Inglis et al., 2008).

### Impact

Our method is not restricted to the values presented here (Table 2), but is applicable to any set of  $x,y$  locations of cells regardless of acquisition method or staining. Also, this method is general in that it can be applied to any arrangement of cells with some underlying vertical organization. The connection with experiments is done via the density map method to characterize microcolumnarity that itself only requires the  $x,y$  coordinates of cells. However, since the initial adjusting parameters come from our density maps, other methods that generate equivalent average measures could conceivably be used as starting parameters to generate the 3D model, such as the one presented by Buxhoeveden et al. (2000a).

The model presented here can also be applied to the construction of virtual dendrite forests using the L-Neuron and ArborVitae programs (Ascoli et al., 2001; Ascoli, 2002) or using other models such as DLA-based diffusive growth mechanisms (Luczak, 2006). In this role, our model can dictate the initial ( $x,y,z$ ) of neuron somata on which to build these networks of dendrites and could include axonal arborizations (Scorcioni and Ascoli, 2005). These generated “forests” can then be used in compartmental neuron simulations to assess the viability of firing and signaling among neurons in the network, similar to other studies that simulate whole-column realistic simulations such as the Blue Brain project (Markram, 2006).

### Software

The code containing the algorithm described in this work to generate 3D configurations given the parameters described in this work is available in the download section of <http://polymer.bu.edu/cruz/micros>.

## Acknowledgments

This work was supported by grants from the National Institutes of Health: R01-AG021133, P01-AG00001 and P51-RR00165.

## References

- Ascoli, G.A., 2002. Neuroanatomical algorithms for dendritic modelling. *Netw. Comput. Neural Syst.* 13 (3), 247–260.
- Ascoli, G.A., Krichmar, J.L., Scorcioni, R., Nasuto, S.J., Senft, S.L., 2001. Computer generation and quantitative morphometric analysis of virtual neurons. *Anat. Embryol.* 204 (4), 283–301.
- Benes, F.M., Bird, E.D., 1987. An analysis of the arrangement of neurons in the cingulate cortex of schizophrenic patients. *Arch. Gen. Psychiatry* 44 (7), 608–616.
- Buldryev, S.V., Cruz, L., Gomez-Isla, T., Gomez-Tortosa, E., Havlin, S., Le, R., Stanley, H.E., Urbanc, B., Hyman, B.T., 2000. Description of microcolumnar ensembles in association cortex and their disruption in Alzheimer and Lewy body dementias. *Proc. Natl. Acad. Sci.* 97 (10), 5039–5043.
- Buxhoeveden, D.P., Casanova, M.F., 2002a. The minicolumn hypothesis in neuroscience. *Brain* 125, 935–951.
- Buxhoeveden, D.P., Casanova, M.F., 2002b. The minicolumn and Evolution of the Brain. *Brain Behav. Evol.* 60, 125–151.
- Buxhoeveden, D., Casanova, M.F., 2005. Encephalization, minicolumns, and hominid evolution. In: Casanova, M.F. (Ed.), *Neocortical modularity and the cell minicolumn*. New York, Nova Science Publishers, pp. 117–136.
- Buxhoeveden, D.P., Switala, A.E., Roy, E., Casanova, M.F., 2000a. Quantitative analysis of cell columns in the cerebral cortex. *J. Neurosci. Methods* 97, 7–17.
- Buxhoeveden, D., Roy, E., Switala, A., Casanova, M.F., 2000b. Reduced interneuronal space in schizophrenia. *Biol. Psychiatry* 47, 681–682.
- Buxhoeveden, D.R., Switala, A.E., Litaker, M., Roy, E., Casanova, M.F., 2001. Lateralization of minicolumns in human planum temporale is absent in nonhuman primate cortex. *Brain, Behavior and Evolution* 57 (6), 349–358.
- Buxhoeveden, D., Fobbs, A., Roy, E., Casanova, M., 2002. Quantitative comparison of radial cell columns in children with down's syndrome and controls. *J. Intellect. Disabil. Res.* 46, 76–81 Part I.
- Casanova, M.F., Buxhoeveden, D.P., Cohen, M., Switala, A.E., Roy, E.L., 2002. Minicolumnar pathology in dyslexia. *Ann. Neurol.* 52 (1), 108–110.
- Casanova, M.F., Buxhoeveden, D., Gomez, J., 2003. Disruption in the inhibitory architecture of the cell minicolumn: Implications for autism. *Neuroscientist* 9 (6), 496–507.
- Constantinidis, C., Franowicz, M.N., Goldman-Rakic, P.S., 2001. Coding specificity in cortical microcircuits: a multiple-electrode analysis of primate prefrontal cortex. *J. Neurosci.* 21, 3646–3655.
- Cruz, L., Roe, D.L., Urbanc, B., Cabral, H., Stanley, H.E., Rosene, D.L., 2004. Age-related reduction in microcolumnar structure in area 46 of the rhesus monkey correlates with behavioral decline. *Proc. Natl. Acad. Sci.* 101, 15846–15851.
- Cruz, L., Buldyrev, S.V., Peng, S., Roe, D.L., Urbanc, B., Stanley, H.E., Rosene, D.L., 2005. A statistically based density map method for identification and quantification of regional differences in microcolumnarity in the monkey brain. *Journal of Neuroscience Methods* 141, 321–332.
- DeFelipe, J., Hendry, S.H.C., Hashikawa, T., Molinari, M., Jones, E.G., 1990. A microcolumnar structure of monkey cerebral-cortex revealed by immunocytochemical studies of double bouquet cell axons. *Neuroscience* 37, 655–673.
- Gabbott, P.L.A., 2003. Radial organization of neurons and dendrites in human cortical areas 25, 32, and 32'. *Brain Res.* 992, 298–304.
- Helmstaedter, M., de Kock, C.P.J., Feldmeyer, D., Bruno, R.M., Sakmann, B., 2007. Reconstruction of an average cortical column in silico. *Brain Res. Rev.* 55, 193–203.
- Hendry, S.H.C., Schwark, H.D., Jones, E.G., Yan, J., 1987. Numbers and proportions of GABA-immunoreactive neurons in different areas of monkey cerebral cortex. *J. Neurol.* 7, 1503–1519.
- Horton, J.C., Adams, D.L., 2005. The cortical column: a structure without a function. *Phil. Trans. R. Soc. B* 360, 837–862.
- Inglis, A., Cruz, L., Roe, D.L., Stanley, H.E., Rosene, D.L., Urbanc, B., 2008. Automated retrieval of neuron location from Nissl-stained tissue. *J. Microsc.* 230 (3).
- Jones, E.G., 2000. Microcolumns in the cerebral cortex. *Proc. Natl. Acad. Sci.* 97 (10), 5019–5021.
- Krieger, P., Kuner, T., Sakmann, B., 2007. Synaptic connections between layer 5B pyramidal neurons in mouse somatosensory cortex are independent of apical dendrite bundling. *J. Neurosci.* 27, 11473–11482.
- Lev, D.L., White, E.L., 1997. Organization of pyramidal cell apical dendrites and composition of dendritic clusters in the mouse: emphasis on primary motor cortex. *Eur. J. Neurosci.* 9 (2), 280–290.
- Luczak, A., 2006. Spatial embedding of neuronal trees modeled by diffusive growth. *J. Neurosci. Methods* 157 (1), 132–141.
- Markram, H., 2006. Blue brain project. *Nat. Rev. Neurosci.* 7 (2), 153–160.
- Mountcastle, V.B., 1957. Modality and topographic properties of single neurons of cat's somatic sensory cortex. *J. Neurophysiol.* 20, 408–434.
- Mountcastle, V.B., 1997. Columnar organization of the neocortex. *Brain* 120, 701–722.
- Mountcastle, V.B., 2003. Untitled—introduction. *Cereb. Cortex* 13 (1), 2–4.
- Peters, A., 1994. The organization of the primary visual cortex in the macaque. In: Peters, A., Rockland, K.S. (Eds.), *Cerebral cortex*, 10. Plenum Press, New York, pp. 1–35.
- Peters, A., Kara, D.A., 1987. Neuronal composition of area 17 of rat visual cortex: IV. The organization of pyramidal cells. *J. Comp. Neurol.* 260 (4), 573–590.
- Peters, A., Sethares, C., 1991. Organization of pyramidal neurons in area-17 of monkey visual-cortex. *J. Comp. Neurol.* 306 (1), 1–23.
- Peters, A., Sethares, C., 1996. Myelinated axons and the pyramidal cell modules in monkey primary visual cortex. *J. Comp. Neurol.* 365 (2), 232–255.
- Peters, A., Cifuentes, J.M., Sethares, C., 1997. The organization of pyramidal cells in area 18 of the rhesus monkey. *Cereb. Cortex* 7, 405–421.
- Rockland, K.S., Ichinohe, N., 2004. Some thoughts on cortical minicolumns. *Exp. Brain Res.* 158, 265–277.
- Saleem, K.S., Tanaka, K., Rockland, K.S., 1993. Specific and columnar projection from area TEO to TE in the macaque inferotemporal cortex. *Cerebral Cortex* 3 (5), 454–464.
- Scorcioni, R., Ascoli, G.A., 2005. Algorithmic reconstruction of complete axonal arborizations in rat hippocampal neurons. *Neurocomputing* 65–66, 15–22.
- Skoglund, T.S., Pascher, R., Berthold, C.H., 2004. Aspects of the organization of neurons and dendritic bundles in primary somatosensory cortex of the rat. *Neurosci. Res.* 50 (2), 189–198.
- Tommerdahl, M., Favorov, O., Whitsel, B.L., Nakhle, B., Gonchar, Y.A., 1993. Minicolumnar activation patterns in cat and monkey SI cortex. *Cereb. Cortex* 3 (5), 399–411.
- Urbanc, B., Cruz, L., Le, R., Sanders, J., Hsiao Ashe, K., Duff, K., Stanley, H.E., Irizarry, M.C., Hyman, B.T., 2002. Neurotoxic effects of thioflavin S-positive amyloid deposits in transgenic mice and Alzheimer's disease. *Proc. Natl. Acad. Sci.* 99 (22), 13990–13995.
- VanHoesen, G.W., Solodkin, A., 1993. Some modular features of temporal cortex in humans as revealed by pathological-changes in Alzheimer's disease. *Cereb. Cortex* 3 (5), 465–475.
- Vercelli, A.E., Garbossa, D., Curtetti, R., Innocenti, G.M., 2004. Somatodendritic minicolumns of output neurons in the rat visual cortex. *Eur. J. Neurosci.* 20 (2), 495–502.
- White, E.L., Peters, A., 1993. Cortical modules in the posteromedial barrel subfield (SML) of the mouse. *J. Comp. Neurol.* 334, 86–96.